

# Energetics of a Strongly pH Dependent RNA Tertiary Structure in a Frameshifting Pseudoknot

Paul L. Nixon and David P. Giedroc\*

Department of Biochemistry  
and Biophysics, Center for  
Macromolecular Design, Texas  
A&M University, College  
Station, TX 77843-2128, USA

Retroviruses employ  $-1$  translational frameshifting to regulate the relative concentrations of structural and non-structural proteins critical to the viral life cycle. The 1.6 Å crystal structure of the  $-1$  frameshifting pseudoknot from beet western yellows virus reveals, in addition to Watson-Crick base-pairing, many loop-stem RNA tertiary structural interactions and a bound  $\text{Na}^+$ . Investigation of the thermodynamics of unfolding of the beet western yellows virus pseudoknot reveals strongly pH-dependent loop-stem tertiary structural interactions which stabilize the molecule, contributing a net of  $\Delta H \approx -30 \text{ kcal mol}^{-1}$  and  $\Delta G_{37}^\circ$  of  $-3.3 \text{ kcal mol}^{-1}$  to a total  $\Delta H$  and  $\Delta G_{37}^\circ$  of  $-121$  and  $-16 \text{ kcal mol}^{-1}$ , respectively, at pH 6.0, 0.5 M  $\text{K}^+$  by DSC. Characterization of mutant RNAs supports the presence of a  $\text{C8}^+ \cdot \text{G12} \cdot \text{C26}$  loop 1-stem 2 base-triple ( $\text{pK}_a = 6.8$ ), protonation of which contributes nearly  $-3.5 \text{ kcal mol}^{-1}$  in net stability in the presence of a wild-type loop 2. Substitution of the nucleotides in loop 2 with uridine bases, which would eliminate the minor groove triplex, destroys pseudoknot formation. An examination of the dependence of the monovalent ion and type on melting profiles suggests that tertiary structure unfolding occurs in a manner quantitatively consistent with previous studies on the stabilizing effects of  $\text{K}^+$ ,  $\text{NH}_4^+$  and  $\text{Na}^+$  on other simple duplex and pseudoknotted RNAs.

© 2000 Academic Press

\*Corresponding author

Keywords: RNA; thermodynamics; pseudoknot; frameshifting; energetics

## Introduction

Translational frameshifting is an important mechanism utilized by retroviruses and other RNA viruses to regulate the synthesis of structural proteins relative to replicative enzymes (for reviews, see Farabaugh, 1993; Gesteland & Atkins, 1996; Matsufuji *et al.*, 1996). While frameshifting can occur in the  $-1$ ,  $-2$  and  $+1$  frames, the  $-1$  frameshift is clearly one of the most common and best understood. Specifically,  $-1$  frameshifting is frequently observed between the overlapping *gag* and *pro* reading frames in RNA viruses and results in the production of a *gag-pro* polyprotein which is packaged and processed in the mature virus particle. The efficiency of the  $-1$  frameshift event regulates the relative concentrations of the *gag* and *pro* proteins at a level appropriate to efficient viral infectivity (Brierley *et al.*, 1989), and alteration of

frameshifting efficiencies has been shown to inhibit viral and retroviral propagation (Dinman *et al.*, 1997; Hung *et al.*, 1998). Thus,  $-1$  frameshifting is an excellent system to systematically study the mechanism of translational recoding in viral protein expression.

Previous studies suggest that efficient  $-1$  frameshifting requires the presence of specific features in the ribosomally translated mRNA. These features include a "slippery site" with the specific sequence X XXY YYZ where XXY is read in the zero frame and XXX is read in the  $-1$  frame and a downstream ( $3'$  to the slip site) RNA structure such as a pseudoknot (Gesteland & Atkins, 1996), stable hairpin (Kang, 1998), or three helical junction (Rettberg *et al.*, 1999). The most commonly observed structure is an H-type (hairpin-type) pseudoknot formed when the loop region of an RNA stem-loop structure base-pairs with an adjacent single-stranded region (Pleij *et al.*, 1985; Wyatt *et al.*, 1990). While the pseudoknot structure has been shown to be necessary for efficient frameshifting, it is not sufficient in itself and must be optimally positioned six to eight nucleotides downstream of a slippery sequence (Farabaugh,

Abbreviations used: H-type, hairpin-type; BWYV, beet western yellows virus; DSC, differential scanning calorimetry; PK, pseudoknotted intermediate.

E-mail address of the corresponding author: giedroc@tamu.edu

1996). Although the presence and identity of the downstream pseudoknot has been observed to greatly enhance the efficiency of frameshifting at the slip site, correlations between frameshifting efficiency, pseudoknot stability, and pseudoknot structure are only beginning to be understood (Gesteland & Atkins, 1996).

In addition to their role in translational regulation, RNA pseudoknots can be considered to be one of the most simple RNA folds (Pleij *et al.*, 1985) and function as basic building blocks of more complex folded RNAs. The H-type pseudoknot should be able to support a diversity of stabilizing tertiary interactions. The two helical stems connected by a continuous strand may be in an extended conformation, coaxially stacked, or separated by an extrahelical or intercalated intervening nucleotide. While stem-stem interactions such as coaxial stacking and intercalated nucleotides were previously observed in autoregulatory and frameshifting pseudoknots (Du *et al.*, 1996, 1997; Holland *et al.*, 1999; Chen *et al.*, 1996), two recent structures, a crystal structure (Su *et al.*, 1999) of the frameshift pseudoknot from the plant luteovirus, beet western yellows virus (BWYV), and the NMR solution structure of the 3'-terminal pseudoknot of the tobacco yellow mosaic virus tRNA-like region (Kolk *et al.*, 1998) have revealed observable loop-stem interactions.

Obtaining a molecular understanding of the specific interactions that a pseudoknot can form, as well as the contributions that those interactions make to the stability and function of the molecule, is essential to the accurate prediction of pseudoknots from RNA sequence and central to understanding the role that RNA pseudoknots play in  $-1$  ribosomal frameshifting. Previous thermodynamic analysis of the energetics of unfolding of several pseudoknots suggests that if defined loop-stem interactions do exist, these interactions do not contribute greatly to the enthalpic stability of the molecule (Gluick *et al.*, 1997; Theimer *et al.*, 1998; Nixon & Giedroc, 1998; Theimer & Giedroc, 1999). However, the loop-stem tertiary-structural interactions observed in the crystal structure of the BWYV pseudoknot are far more extensive than observed to date in other H-type pseudoknots, and some of them have not been previously observed in other folded RNAs (Figure 1).

Of special interest is the C8·G12-C26 base-triple formed by a loop 1-stem 2 interaction (red), the loop 2-stem 1 interactions where loop 2 forms a minor groove triplex with stem 1 (blue), a Na<sup>+</sup> (yellow), and the rather unusual positioning of the A25 and U13 nucleotides which would be predicted to form a closing base-pair of stem 2 at the helical junction of the two stems (green) (Figure 1). This structure suggests the possibility that the BWYV pseudoknot may derive significant stabilization from these interactions and makes testable predictions about the extent to which non-canonical loop-stem interactions contribute to the stability of this molecule.

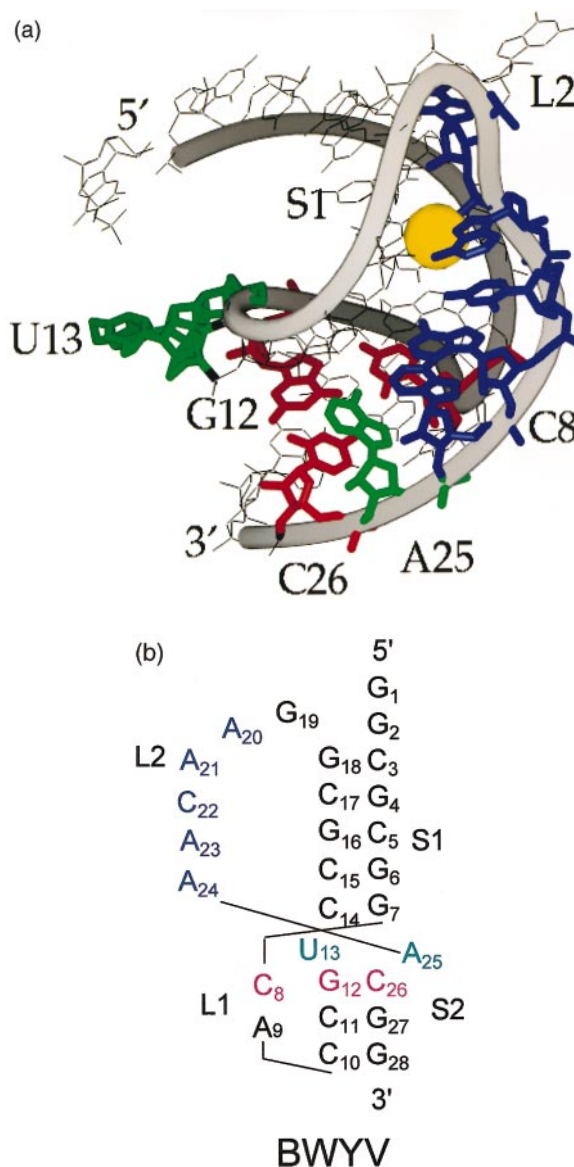


**Figure 1.** (a) The BWYV pseudoknot structure as determined by X-ray crystallography (Su *et al.*, 1999) (PDB code 437D). The C8·G12·C26 base-triple interaction is shown in red and the loop 2 nucleotides that make crystal contacts with stem 1 are in blue. Also shown are U13 and A25 which would be predicted to form a base-pair in stem 2 (green) and a Na<sup>+</sup> bound between loop 2 and stem 1 nucleotides (yellow). (b) Schematic of the secondary structure of the BWYV pseudoknot with the corresponding nucleotides from (a) colored for clarity.

Here, we describe an investigation of the thermodynamics of unfolding for the BWYV pseudoknot focusing on the role that the loop-stem interactions observed in the crystal structure contribute to the stability of the pseudoknot in solution. We find that these interactions make a substantial enthalpic contribution to the stability of the molecule, in marked contrast to thermodyn-

amic studies conducted on other H-type pseudoknots (Gluck *et al.*, 1997; Theimer *et al.*, 1998; Nixon & Giedroc, 1998; Theimer & Giedroc, 1999). Characterization of wild-type and mutant RNAs supports the presence of a C8<sup>+</sup>·G12-C26 base-triple ( $pK_a = 6.8$ ) in which C8 is protonated at N3 to form a H-bond to the O6 of G12. The pseudoknot is destabilized to a point below that of the component stem 1 hairpin when loop 2-stem 1 interactions are lost or when the C8<sup>+</sup>·G12-C26 base-triple is replaced by a potentially non-cognate U8·A12-U26 substitution. Investigation of the monovalent ion dependence of the unfolding of the BWYV pseudoknot indicates little or no preference for the monovalent ions Na<sup>+</sup>, K<sup>+</sup> or NH<sub>4</sub><sup>+</sup>, which would seem to argue against a specifically bound Na<sup>+</sup> linked to the stability of the molecule.

## Results

### BWYV pseudoknot unfolds in three steps with the first unfolding transition attributed to tertiary structure

The thermal unfolding of complex RNA molecules can be modeled thermodynamically as a series of coupled equilibria corresponding to sequential interacting unfolding transitions (Gluck *et al.*, 1997; Theimer *et al.*, 1998; Nixon & Giedroc, 1998; Theimer & Giedroc, 1999; Laing & Draper, 1994; Gluck & Draper, 1994). To better understand the contributions of the interactions observed in the structure of the fully folded BWYV pseudoknot, we have employed a number of techniques to analyze the energetics of unfolding of this RNA. From theory, the secondary structure predicts two unfolding helix-to-coil transitions with the ratio of the hyperchromicity ( $\partial A/\partial T$ ) at 260 nm and 280 nm ( $A_{260}/A_{280}$ ) less than one (favoring 280) (Fresco *et al.*, 1963). The shorter helical stem 2 is predicted to unfold with a van't Hoff enthalpy of 25 kcal mol<sup>-1</sup> if U13 and A25 are unpaired and 33 kcal mol<sup>-1</sup> if they are paired (Figure 1). Stem 1 is predicted by improved nearest neighbor and hydrogen bonding (INN-HB) rules (Xia *et al.*, 1998) to denature with a total enthalpy of 50 kcal mol<sup>-1</sup> for the helical segment alone not including any contributions from 3' stacking of loop residues. Thus, the total  $\Delta H$  observed due to secondary structure unfolding is expected to be on the order of 75 to 83 kcal mol<sup>-1</sup>.

Since the BWYV pseudoknot may have a protonated cytosine (C8), melting profiles were collected over a wide range of pH. The top row of Figure 2 shows the melting profiles of the BWYV pseudoknot at pH 6.0, 7.0, and 8.0 in the presence of 0.5 M K<sup>+</sup> (left to right). By optical spectroscopy, the BWYV pseudoknot clearly unfolds *via* two intermediates in three distinct unfolding transitions at all pH's tested (Figure 2, top row). All attempts to fit these data to two unfolding transitions resulted in large non-random deviations in the residuals and comparatively large  $\chi^2$  values associ-

ated with a visibly poor fit. The residuals improve dramatically and assume a more random distribution upon introduction of a third unfolding transition with an associated improvement in the values of  $\chi^2$  (see Materials and Methods). Differential scanning calorimetry (DSC) data corroborate the presence of three rather than two unfolding transitions since significantly more calorimetric enthalpy is recovered than can be attributed to secondary structure alone (Figure 2, bottom row). Van't Hoff analysis of these calorimetric melting profiles returns transition enthalpies and  $t_m$  values which agree very well with the values obtained from deconvolution of the optical melts (Table 1). At pH 7.0, the sum of the van't Hoff enthalpies calculated from the optical melting profile is 115(±13) kcal mol<sup>-1</sup> and shows excellent agreement with the calorimetrically determined total enthalpy of unfolding of 121(±2) kcal mol<sup>-1</sup>. These two values are identical within experimental error and verify the presence of a large enthalpic contribution ( $\geq 30$  kcal mol<sup>-1</sup>) to the unfolding of the molecule apart from that predicted by its secondary structure. Additionally, the close agreement of the calorimetry and optical spectroscopy provides strong evidence that the melting profiles are well approximated by the sequential two-state equilibrium unfolding model (Laing & Draper, 1994).

### Assignment of unfolding transitions to molecular unfolding events

The INN-HB rules (Xia *et al.*, 1998) predict that the unfolding of the S1 hairpin (five base-pair stem and six nucleotide loop) in the absence of any other structure should occur with a  $\Delta H$  of 50 kcal mol<sup>-1</sup> at 89.0°C and a hyperchromic ratio (Fresco *et al.*, 1963) ( $A_{260}/A_{280}$ ) of less than 1. These parameters show excellent agreement with the last unfolding transition (S1 → U). The other two transitions are expected to correspond to the unfolding of helical of stem 2 and the tertiary structure. Due to the simplicity of the molecule, it is unlikely that the tertiary structure could be formed in the absence of a fully folded stem 2, consistent with studies on another RNA pseudoknot (Gluck & Draper, 1994). The resolved enthalpies and hyperchromic signatures lead us to propose that unfolding of the tertiary structure occurs first ( $\Delta H = 32(\pm 7)$  kcal mol<sup>-1</sup>) leaving a pseudoknotted intermediate (PK) with no defined loop-stem structural interactions. The second transition ( $\Delta H = 29(\pm 2)$  kcal mol<sup>-1</sup>) would therefore correspond to the unfolding of the less stable of the two stems, stem 2 (PK → S1), predicted to occur with a  $\Delta H$  of 26 or 33 kcal mol<sup>-1</sup> depending on whether the closing base-pair (U13-A25) in stem 2 is formed (Figure 1). This leaves a stem 1 hairpin intermediate (S1), which denatures ( $\Delta H = 55(\pm 2)$  kcal mol<sup>-1</sup>) to give random coil RNA (U). Thus, the proposed equilibrium unfolding pathway is F ↔ PK ↔ S1 ↔ U (Figure 3).

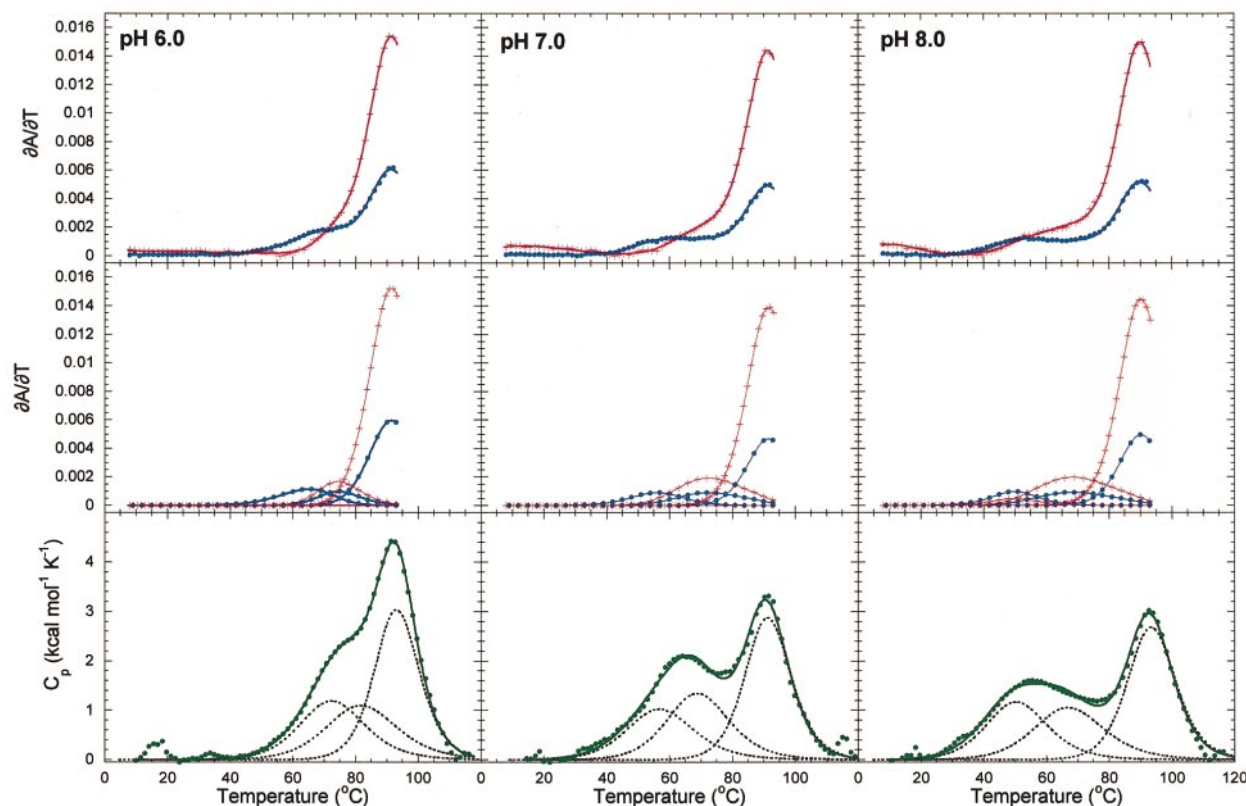


**Figure 2.** Representative melting profiles of the BWYV pseudoknot collected in 0.5 M  $K^+$  at the pH value indicated. The top row shows every fifth data point of the dual wavelength optical denaturation profiles collected at 260 (●) and 280 (+) nm wavelengths as described in Materials and Methods. Superimposed on the data is the composite fit calculated from the individual thermodynamic transitions observed for the RNA. The middle row shows the individual transitions which are deconvoluted from the data on the top row. The bottom row shows representative DSC scans collected under the same conditions as the optical data at concentrations of 40.1, 34.8 and 39.5  $\mu\text{M}$ , respectively. The data shown in these panels represent five percent of the actual data and has both the composite fit and the individual transitions superimposed on the data. The calculated parameters from these fits are compiled in Table 1.

### The stability of the BWYV pseudoknot is strongly pH dependent

In the crystal structure, C8 in loop 1 and the G12-C26 base-pair in stem 2 form a well-defined, non-canonical base-triple interaction (Figure 1, red). This base-triple may be further stabilized by an additional hydrogen bond from A25 to create a base-quadruple (Su *et al.*, 1999). This C8·G12-C26 base-triple would be expected to have some very distinct thermodynamic features. For example, a deprotonated C8 can form two hydrogen bonds to the G12-C26 base-pair, while a protonated C8 can potentially form three H-bonds thereby stabilizing a  $\text{C8}^+\cdot\text{G12-C26}$  triple interaction. Since the predicted C8  $\text{N3}^+\text{H}$  to G12 O6 H-bond should display a pH dependence if present in the base-triple and protonated near neutral pH, the melting profiles of the wild-type RNA should be strongly pH-dependent if this interaction contributes significantly to the stability of the molecule.

Strikingly, the wild-type pseudoknot exhibits a marked stabilization as a function of pH at 0.5 M  $K^+$ . At pH 6.0 (Figure 2, left), the  $t_m$  for tertiary

structure unfolding ( $F \rightarrow \text{PK}$ ) occurs at higher temperature as the pH is lowered, while higher pH destabilizes the pseudoknot (Figure 2, right). Since  $\Delta H$  for unfolding of the tertiary structure is largely independent of pH, a plot of  $t_m^{-1}$  versus  $[\text{H}^+]$  was fit to equation (1) to determine the  $\text{p}K_a$  of the protonation event (Figure 4):

$$\frac{1}{t_{\text{mobs}}} = \frac{1}{t_{\text{m0}}} + \left( \frac{1}{t_{\text{m1}}} + \frac{1}{t_{\text{m0}}} \right) \frac{[\text{H}^+]K_a}{1 + [\text{H}^+]K_a} \quad (1)$$

where  $t_{\text{m0}}$  and  $t_{\text{m1}}$  are the  $t_m$  of the deprotonated and protonated RNAs in degrees K and  $K_a$  is the association constant ( $\text{M}^{-1}$ ) of the RNA for this proton.

The resolved values are  $t_{\text{m0}} = 47.2(\pm 0.3)^\circ\text{C}$ ,  $t_{\text{m1}} = 75.2(\pm 0.6)^\circ\text{C}$  with the  $\text{p}K_a = 6.8(\pm 0.1)$ . If this correlates to the N3 proton of C8, then this represents significant elevation from the  $\text{p}K_a$  for free cytosine ( $\text{p}K_a = 4.5$ ) (Saenger, 1984). An approximation of the total stabilization derived from this protonation event can be calculated directly by comparing  $\Delta G_{37}^\circ$  at pH 6.0 and pH 8.0 since the pseudoknot appears fully stabilized at pH 6.0 and

**Table 1.** Thermodynamic parameters for the unfolding of the wild-type BWYV pseudoknot as a function of pH

		$\Delta H$ (kcal mol <sup>-1</sup> )	$t_m$ (°C)	$A_{260}/A_{280}$	$\Delta G_{37}^{\circ}$ (kcal mol <sup>-1</sup> )
<b>A. pH 6.0</b>					
Optical <sup>a</sup>	F → PK	25(±3)	70(±2)	260 only	2.3(±0.3)
	PK → S1	35(±8)	81(±4)	<1	4(±1)
	S1 → U	55(±2)	91.2(±0.6)	<1	8.1(±0.3)
	Total	115(±14)			15(±2)
DSC <sup>b</sup>	F → PK	32.7(±0.4)	71.7(±0.3)		3.3(±0.3)
	PK → S1	33.1(±0.6)	82.4(±0.8)		4(±1)
	S1 → U	58(±1)	93.2(±0.1)		8.8(±0.3)
	Total	121(±2)			16(±0.3)
<b>B. pH 7.0</b>					
Optical	F → PK	32(±7)	57.5(±0.5)	260 only	2.0(±0.4)
	PK → S1	29(±2)	74(±2)	<1	3.1(±0.3)
	S1 → U	52.7(±0.2)	90.8(±0.5)	<1	7.8(±0.1)
	Total	114(±10)			13(±1)
DSC	F → PK	29.0(±0.5)	56.4(±0.4)		1.7(±0.4)
	PK → S1	35.4(±0.4)	69.4(±0.3)		3.3(±0.3)
	S1 → U	55.9(±0.2)	91.2(±0.1)		8.3(±0.1)
	Total	121(±1)			13.3(±0.1)
<b>C. pH 8.0</b>					
Optical	F → PK	25(±2)	49(±1)	260 only	1.4(±0.1)
	PK → S1	26(±2)	68(±3)	<1	2.3(±0.2)
	S1 → U	53(±2)	90.6(±0.5)	<1	7.7(±0.3)
	Total	103(±6)			11.5(±0.7)
DSC	F → PK	30.3(±0.3)	49.1(±0.3)		1.1(±0.1)
	PK → S1	31.1(±0.3)	67.6(±0.3)		2.8(±0.2)
	S1 → U	54.2(±0.2)	93.2(±0.1)		8.3(±0.3)
	Total	115.6(±0.8)			12.3(±0.1)

<sup>a</sup> Average of three independent experiments with standard error.

<sup>b</sup> Errors in  $\Delta H$  and  $t_m$  from calorimetry are the errors for the fit only.

<sup>c</sup> Errors reported for  $\Delta G_{37}^{\circ}$  were determined using the percent error associated with  $\Delta H$ .

nearly completely destabilized at pH 8.0. Taking DSC and optical data together,  $\Delta(\Delta G_{37}^{\circ})$  for the F → PK and PK → S1 unfolding steps is 1.6(±0.5) and 1.7(±0.2) kcal mol<sup>-1</sup>, respectively, corresponding to a total  $\Delta G_{37}^{\circ}$  of 3.3 kcal mol<sup>-1</sup> attributed to the protonation of C8. The calculated  $\Delta G_{37}^{\circ}$  from DSC alone is 16.0(±1.0) kcal mol<sup>-1</sup> at pH 6.0 and 12.3(±0.2) kcal mol<sup>-1</sup> at pH 8.0. Subtraction yields a  $\Delta(\Delta G_{37}^{\circ})$  of 3.7(±1.0) kcal mol<sup>-1</sup> attributed to protonation of N3 of C8 as determined calorimetrically. By comparison, the total contribution of stem 2 at pH 8.0 is only 2.8(±0.2) kcal mol<sup>-1</sup> (Table 1).

If the pH-dependence of the melting profile is totally attributable to protonation of C8 N3 to form a C8<sup>+</sup>·G12-C26 base-triple, then substitutions of C8 or the G12-C26 base-pair should abolish the pH dependence. Two mutant RNAs, U8 and A12-U26, were prepared and characterized to test this. Representative optical melting profiles for these two RNAs at pH 7.0, 0.5 M K<sup>+</sup> are shown (Figure 5) with the thermodynamic parameters compiled in Table 2. The  $\Delta G_{37}^{\circ}$  value for tertiary structure unfolding for the A12-U26 mutant (1.4(±0.3) kcal mol<sup>-1</sup>) is identical with that observed for the wild-type pseudoknot at pH 8.0

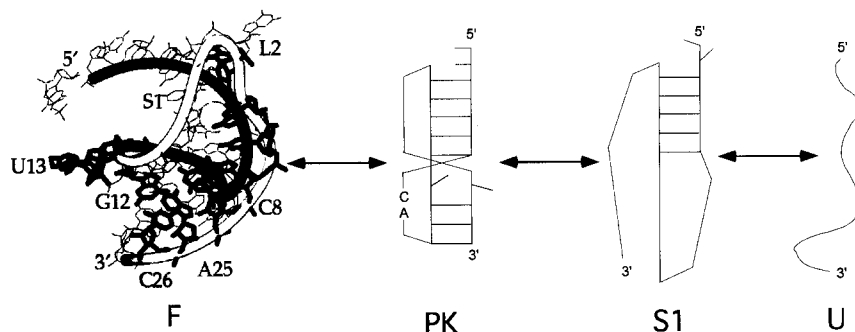


**Figure 3.** Proposed equilibrium unfolding pathway for the BWYV pseudoknot. Denaturation proceeds from the fully folded reference state (F) to PK which is modeled as a pseudoknotted intermediate which lacks tertiary structure. S1 is a folded S1 hairpin intermediate that returns  $\Delta H$  and  $t_m$  values consistent with those expected from the unfolding of the isolated S1 hairpin. U is a random coil achieved upon complete denaturation of the pseudoknot.

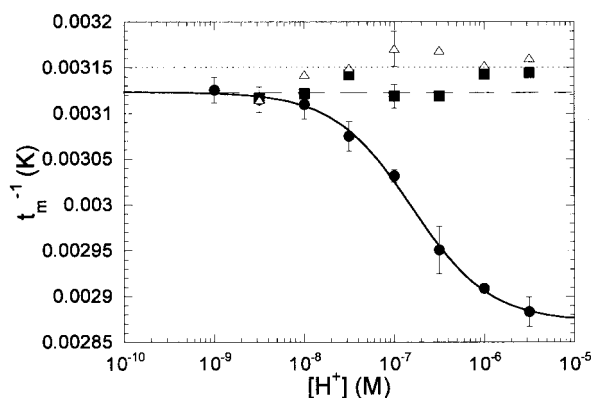


**Figure 4.** The pH dependence of the unfolding of tertiary structure in the BWYV pseudoknot. The  $t_m^{-1}$  for the tertiary structure transition (F  $\rightarrow$  PK) is plotted as a function of  $H^+$  in 0.5 M  $K^+$ . The buffers used are listed in Materials and Methods. Data shown are the (●), wild-type BWYV, (■), A12U26 and (△), U8 mutant RNAs. The wild-type data were fit to equation (1) which describes the dependence of  $t_m^{-1}$  on pH. The two mutants that do not exhibit a pH dependence are shown and illustrate the convergence of the data at high pH. A broken line is drawn corresponding to 49°C and a dotted one at 42°C, the average  $t_m$  values for transition 1 for the A12U26 and U8 mutant RNAs. Data for the wild-type BWYV transition 1 are the average of three independent determinations with the standard error shown. Values reported for A12U26 and U8 RNAs are derived from one or two independent determinations.

(1.4( $\pm$ 0.1) kcal mol $^{-1}$ ). A careful investigation of the pH dependence of the  $t_m$  for transition 1 reveals that the compensatory A12-U26 mutation completely abolishes the pH dependent stabilization of the BWYV pseudoknot (Figure 4). Interest-

ingly, at high pH, the wild-type BWYV pseudoknot appears to possess a stability that is similar to that of the A12-U26 mutant (Figure 4, Table 1) indicating that this mutation does not destabilize the pseudoknot greatly but does alter the energetics and dependence on pH.

A substitution of C8 with a uridine base (U8) potentially replaces one hydrogen bond donor of the base-triple with an acceptor by replacing a C8 N4 amino group with a U8 keto O4 oxygen atom. In addition, the N3 of U8 has an attached imino proton at neutral pH, so no pH dependence would be expected to be observed for this mutant. Like the A12-U26 mutant, the calculated  $\Delta G_{37}^{\circ}$  of 11.3( $\pm$ 0.3) kcal mol $^{-1}$  is strikingly similar to the wild-type pseudoknot at elevated pH with the tertiary structure now contributing only 0.4( $\pm$ 0.1) kcal mol $^{-1}$  to the overall unfolding free energy of the pseudoknot. As expected, the melting profiles observed for this mutant are independent of pH as observed for the A12-U26 substitution (Figure 4), and the total enthalpy of the F  $\rightarrow$  PK unfolding step is similar to that of the wild-type pseudoknot (Table 2). The thermodynamic behavior of these two RNAs is totally consistent with a protonated C8 $^+$ ·G12-C26 base-triple, and additional support for protonation of C8 comes from preliminary  $^1H$  NMR data acquired for the BWYV pseudoknot at pH 6.0 which reveals the presence of a strongly downfield shifted amino group (P.L.N. & D.P.G., unpublished observations).

A third RNA which combines the U8 and A12-U26 substitutions was prepared to determine the effects of a complete loss of the C8 $^+$ ·G12-C26 base-triple interaction when replaced with a potentially non-cognate U8·A12-U26 base-triple interaction. The unfolding of this RNA appears to occur as a single S1  $\rightarrow$  U transition and is modeled accordingly (Figure 6, Table 2). Thus, elimination of the

**Table 2.** Thermodynamic parameters for the unfolding of BWYV pseudoknot mutant RNAs at pH 7.0

		$\Delta H$ (kcal mol $^{-1}$ )	$t_m$ (°C)	$A_{260}/A_{280}$	$\Delta G_{37}^{\circ}$ (kcal mol $^{-1}$ )
A. A12U26					
Optical <sup>a</sup>	F $\rightarrow$ PK	38( $\pm$ 8)	48.8( $\pm$ 0.2)	260 only	1.4( $\pm$ 0.3)
	PK $\rightarrow$ S1	44.0( $\pm$ 0.7)	62( $\pm$ 1)	<1	3.4( $\pm$ 0.1)
	S1 $\rightarrow$ U	47.1( $\pm$ 0.5)	82.7( $\pm$ 0.8)	<1	6.1( $\pm$ 0.1)
	Total	129( $\pm$ 8)			10.8( $\pm$ 0.6)
B. U8					
Optical	F $\rightarrow$ PK	25( $\pm$ 2)	42( $\pm$ 2)	1	0.4( $\pm$ 0.1)
	PK $\rightarrow$ S1	41( $\pm$ 3)	68( $\pm$ 1)	<1	3.7( $\pm$ 0.3)
	S1 $\rightarrow$ U	51.5( $\pm$ 0.5)	87( $\pm$ 2)	<1	7.2( $\pm$ 0.1)
	Total	118( $\pm$ 3)			11.3( $\pm$ 0.3)
DSC <sup>b</sup>	F $\rightarrow$ PK	30.5( $\pm$ 0.4)	46.6( $\pm$ 0.3)		0.9( $\pm$ 0.1)
	PK $\rightarrow$ S1	27.6( $\pm$ 0.3)	68.3( $\pm$ 0.6)		2.5( $\pm$ 0.2)
	S1 $\rightarrow$ U	59.9( $\pm$ 0.3)	86.2( $\pm$ 0.1)		8.2( $\pm$ 0.1)
	Total	115( $\pm$ 1)			11.6( $\pm$ 0.4)
C. U8A12U26					
Optical	F $\rightarrow$ U	53( $\pm$ 1)	88.5( $\pm$ 0.4)	<1	7.7( $\pm$ 0.2)
D. L2U					
Optical	F $\rightarrow$ U	53( $\pm$ 1)	92.4( $\pm$ 0.4)	<1	8.0( $\pm$ 0.2)

<sup>a</sup> Average of three independent experiments with standard error.

<sup>b</sup> Errors in  $\Delta H$  and  $t_m$  from calorimetry are the errors for the fit only.

<sup>c</sup> Errors reported for  $\Delta G_{37}^{\circ}$  were determined using the percent error associated with  $\Delta H$ .

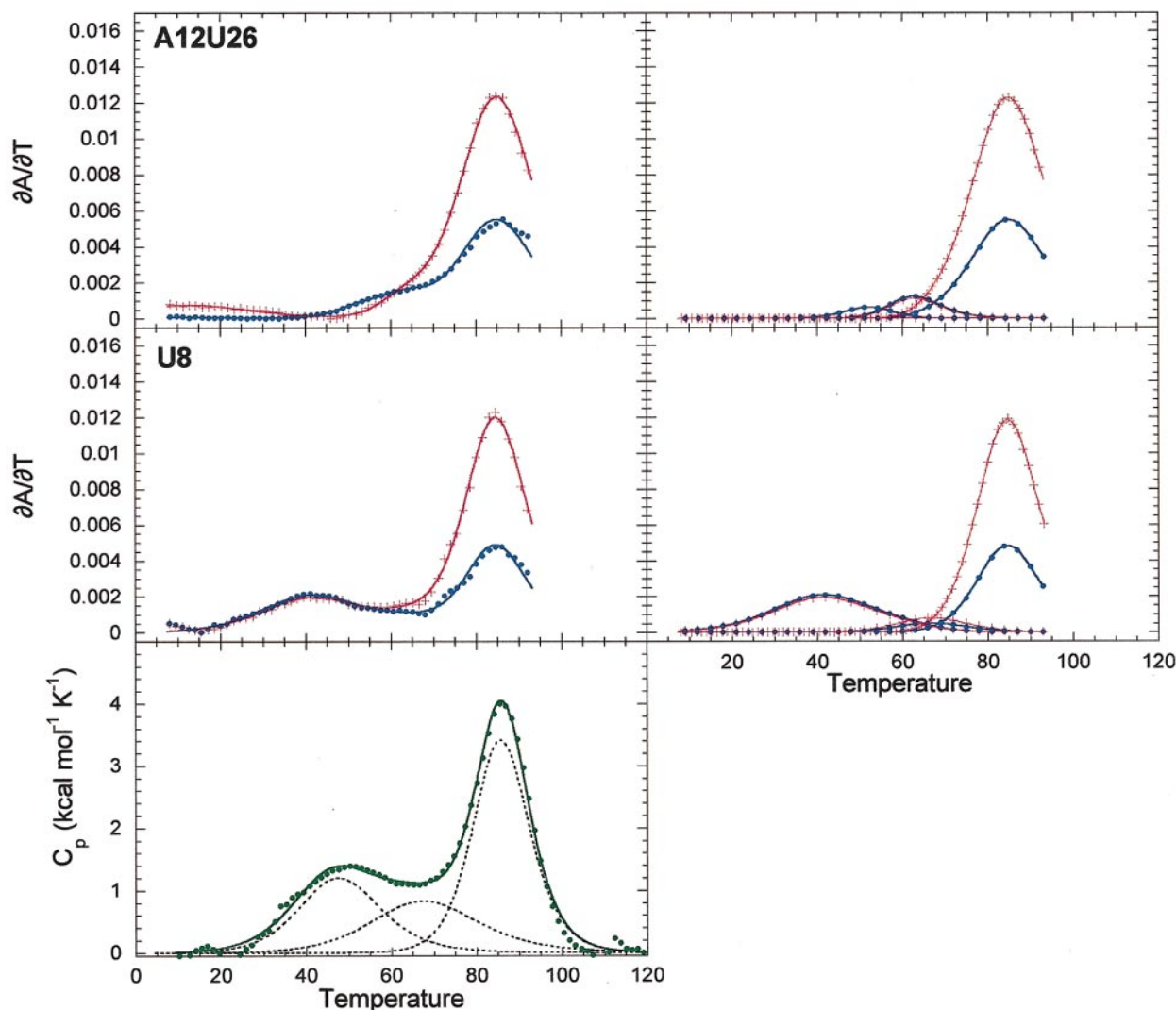


**Figure 5.** Representative melting profiles for the A12U26 and U8 RNAs in 0.5 M  $K^+$  (pH 7.0). In the left-hand panels, every fifth data point for the observed hyperchromic amplitudes at both ( $\bullet$ ), 260 and ( $+$ ), 280 nm are shown with the composite fit superimposed on them. The right-hand panel shows the individual DSC transitions that contribute to the composite fit shown at ( $\bullet$ ), 260 and ( $+$ ), 280 nm. The bottom row shows a DSC scan of the U8 RNA in 0.5 M  $K^+$  (pH 7.0) with an RNA concentration of 55  $\mu$ M. The data shown in this panel represent five percent of the actual data and have both the composite fit and the individual transitions superimposed on the data. The calculated parameters from these fits are compiled in Table 2.

$C8^+ \cdot G12-C26$  base-triple appears to destabilize the pseudoknotted structure to a point below the stability of the S1 hairpin which then becomes the major conformer at equilibrium.

#### Thermodynamic evidence for the stabilizing effects of loop 2-stem 1 interactions

The crystal structure of the BWYV pseudoknot reveals that loop 2 forms an adenosine ladder of novel structure such that the nucleotides in the loop optimize hydrogen bonding with functional groups in the minor groove of stem 1 thereby forming a minor groove triplex (Su *et al.*, 1999). Although present in the crystal structure, the

extent to which these interactions are populated in solution is unknown. If they are, they would be expected to contribute substantially to the stability of the pseudoknotted structure.

To address the presence of thermodynamically stabilizing loop 2-stem 1 base interactions, all of the nucleotides in loop 2 were substituted with a uridine (L2U) which replaces loop 2 with an equivalent length flexible linker (Wyatt *et al.*, 1990). A representative melting profile for the L2U RNA is shown (Figure 6). Although the residuals are clearly non-random (data not shown), the simple interpretation is that the pseudoknot is not or only weakly formed, with the S1 hairpin representing the predominant population of the folded mol-

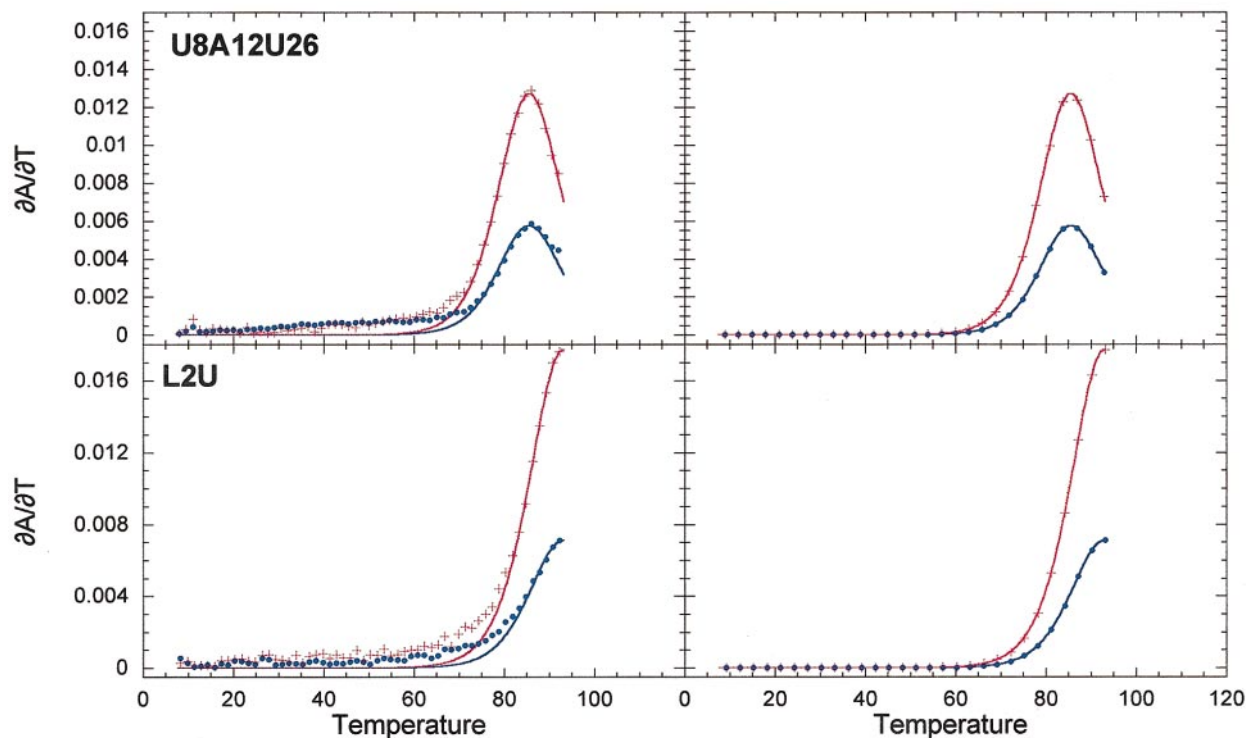


**Figure 6.** Representative melting profiles of the U8A12U26 and L2U mutant RNAs in 0.5 M  $K^+$ , 10 mM Mops (pH 7.0). The left-hand panel shows every fifth data point for the observed hyperchromic amplitudes at both ( $\bullet$ ), 260 and ( $+$ ), 280 nm shown with the composite fit superimposed on them. The right-hand panel shows the individual transitions that contribute to the composite fit shown at ( $\bullet$ ), 260 and ( $+$ ), 280 nm. The calculated parameters from these fits are compiled in Table 2.

ecules (Table 2). Thus, the decrease in stability which results when the loop 2-stem 1 interactions are removed appears sufficient to reduce or even abolish pseudoknot formation to a degree comparable to that of the U8·A12-U26 mutation. This is probably a consequence of the rather weak helical stem 2 in this molecule which appears insufficient to stabilize the pseudoknot in the absence of an intact tertiary structure.

Recent efforts using polymer theory to estimate the global stability of pseudoknots derived from secondary structure predictions (Gulyaev *et al.*, 1999) calculate a  $\Delta G_{37}^\circ$  of  $-6.3 \text{ kcal mol}^{-1}$  for the BWYV pseudoknot if the loops behave as unstructured linkers. This is less than the predicted  $\Delta G_{37}^\circ$  of  $-7.1 \text{ kcal mol}^{-1}$  and experimentally determined  $\Delta G_{37}^\circ$  of  $\sim -8.1 \text{ kcal mol}^{-1}$  for the stem 1 hairpin (Xia *et al.*, 1998). Therefore, in the absence of stabilizing loop-stem interactions, it is perhaps not surprising that the pseudoknot is not the major conformer. Interestingly, while the C8 $^+$ ·G12-C26 base-triple makes a significant contribution to the stability of the pseudoknot, it is not sufficient by itself to drive pseudoknot formation in the absence of the loop 2-stem 1 interactions. This suggests that the energetic penalty for loop closure of a completely unstructured loop 2 overwhelms the energetic gain of base-triple formation, consistent with sig-

nificant cooperativity in the formation of tertiary structure in this pseudoknot.

#### Dependence of the stability of the BWYV pseudoknot on monovalent ions

In the minor groove of stem 1, a  $Na^+$  is proposed to be coordinated by the N3 and 2' OH groups of G16, the *pro*-R<sub>p</sub> phosphate oxygen atom and N7 atom of A21 as well as three water molecules, linking loop 2 with stem 1 (Su *et al.*, 1999). Investigation of the effects of monovalent ion concentration and type on the BWYV pseudoknot melting profile can reveal if monovalent ion binding sites are linked to pseudoknot stability or are specific for one ion relative to another. If the monovalent ion binding site observed crystallographically preferentially binds  $Na^+$ , the  $t_m$  of the tertiary structure and possibly stem 2 unfolding should exhibit a distinct dependence on  $[Na^+]$  relative to other ions. Alternatively, if  $Na^+$  is simply acting as a general counterion to shield phosphate charges, there should be essentially identical behavior for all monovalent ions tested, in a manner generally consistent with polyelectrolyte theory.

Melting profiles were collected for the wild-type BWYV pseudoknot from 0.050 to 0.750 M for NaCl, KCl, and  $NH_4Cl$  and the data plotted in the form of  $t_m^{-1}$  versus  $\ln [M^+]$  for the wild-type pseu-

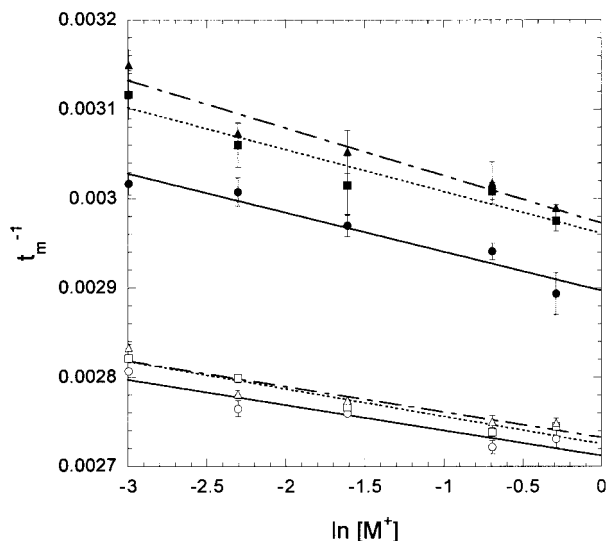


**Figure 7.** Dependence of the stabilities of the tertiary structure (F → PK) and the S1 hairpin (S1 → U) transitions on monovalent ion type.  $t_m^{-1}$  for the first (filled symbols) and last (open symbols) transitions are plotted as a function of ionic strength for ( $\blacktriangle$ ,  $\triangle$ ),  $K^+$ ; ( $\blacksquare$ ,  $\square$ ),  $Na^+$  and ( $\bullet$ ,  $\circ$ ),  $NH_4^+$ . The continuous line represents fits to equation (2) used to calculate  $\Delta n$ . See the text for details.

doknot tertiary transition and the S1 hairpin unfolding transition (Figure 7). As can be seen, these data can be fit to a straight line with the slopes of the F → PK transition essentially independent of the identity of  $M^+$ . Knowledge of  $\Delta H$  for the transition allows application of equation (2) to estimate  $\Delta n$ , the apparent number of delocalized  $M^+$  released upon each unfolding step (Laing *et al.*, 1994):

$$\frac{\partial t_m^{-1}}{\partial \ln[M^+]} = \frac{-R\Delta n}{\Delta H} \quad (2)$$

where  $R$  is the gas constant,  $\Delta n$  is the apparent number of counter ions released, and  $\Delta H$  is the enthalpy of the transition. The  $\Delta n$  for the tertiary unfolding transition is  $0.7(\pm 0.1)$ ,  $0.7(\pm 0.1)$  and  $0.8(\pm 0.1)$  for  $K^+$ ,  $Na^+$  and  $NH_4^+$ , respectively. These values are identical to one another. For comparison, calculated values of  $\Delta n$  are  $0.8(\pm 0.1)$ ,  $0.7(\pm 0.1)$  and  $0.8(\pm 0.1)$  for stem 2 unfolding and  $0.7(\pm 0.1)$ ,  $0.8(\pm 0.1)$  and  $0.7(\pm 0.1)$  for the stem 1 unfolding transition in  $K^+$ ,  $Na^+$  and  $NH_4^+$ , respectively. Although the molecular significance of  $\Delta n$  is unclear from these studies alone (*cf.* Laing *et al.*, 1994), the relative magnitudes of  $\Delta n$  allow us to reach two important conclusions. One is that when normalized for the number of phosphates which are modeled to participate in each unfolding transition (Figure 3), the sensitivity of tertiary structure (F → PK) unfolding to monovalent ion concentration is significantly greater than is PK → S1 hairpin unfolding, which itself is more sensitive

than the S1 hairpin → U transition. This is the expected trend if the negative charge density is significantly greater in the F versus PK versus S1 hairpin states and is consistent with previous studies which have analyzed the mono- and multivalent ion concentration dependence of pseudoknot unfolding transitions (Gluck *et al.*, 1997; Nixon *et al.*, 1999). Secondly, the similarity of the calculated values of  $\Delta n$  for tertiary structure unfolding makes it unlikely that a  $Na^+$  ion preferentially contributes to the stability of the molecule over other monovalent ions. Although there is an observable trend in  $t_m$  at any one  $[MCl]$  which slightly favors  $NH_4^+$  over  $Na^+$  or  $K^+$ , this trend is not specific to tertiary structure unfolding and is qualitatively consistent with the results of previous studies on the MuLV and MMTV read-through pseudoknots (Gluck *et al.*, 1997; Theimer & Giedroc, 2000).

## Discussion

The BWYV frameshifting pseudoknot is stabilized by tertiary interactions apart from Watson-Crick base-pairing and base-stacking which total  $-30 \text{ kcal mol}^{-1}$  in  $\Delta H$ . Surprisingly, the magnitude of this stabilization is comparable to that present in more highly folded RNAs that have been both structurally and thermodynamically characterized. For example, tertiary structure formation in the 58 nucleotide L11 ribosomal RNA fragment contributes a net  $\Delta H$  of  $-23 \text{ kcal mol}^{-1}$  in the absence of a specifically bound  $NH_4^+$  and  $\geq 50 \text{ kcal mol}^{-1}$  in its presence (Laing & Draper, 1994). Temperature gel gradient electrophoresis experiments (Szewczak *et al.*, 1998) on the 168 nt *Tetrahymena thermophila* group I intron P4-P6 domain reveal that the extensive tertiary contacts in this RNA contribute approximately  $-28(\pm 3) \text{ kcal mol}^{-1}$  of stabilizing enthalpy. Thus, the BWYV pseudoknot contains a net stabilizing enthalpy which is comparable in magnitude to that associated with these much larger and highly folded RNAs (Cate *et al.*, 1996; Conn *et al.*, 1999) and greatly exceeds that present in other H-type and frameshifting pseudoknots where secondary structure accounts for nearly all of the folding enthalpy.

Since little or no change in net  $\Delta H$  is observed in the loop 1-stem 2 mutant RNAs, a large fraction of the observed enthalpy of tertiary structural unfolding may well derive from loop 2-stem 1 interactions. A21, C22 and A23 are observed to be stacked in the crystal structure (Su *et al.*, 1999), and A20, although making lattice contacts in the crystal, may be stacked in solution. Previous studies have shown that stacking in single-stranded poly(A) can contribute  $\sim -3.0\text{-}3.4 \text{ kcal mol}^{-1}$  of enthalpy per stacking interaction (Filimonov & Privalov, 1978; Breslauer & Sturtevant, 1977). In addition to these stacking interactions, loop 2 is predicted to form  $\sim 16$  H-bonds to itself and to functional groups in stem 1. In a recent study (Silverman & Cech, 1999), a reciprocal pair of H-

bonds between 2'-OH groups in the ribose zipper moiety of the *Tetrahymena thermophila* P4-P6 domain have been estimated to contribute  $-1 \text{ kcal mol}^{-1} \Delta G_{35}^{\circ}$ . The contribution of each H-bond appears to be approximately additive, displaying little or no cooperativity, suggesting that each individual H-bond in an RNA tertiary structure may contribute as much as  $-0.4$  to  $-0.5 \text{ kcal mol}^{-1} \Delta G_{35}^{\circ}$  to the stability. Thus, stacking and H-bonding interactions associated with loop 2 may well be the primary source of the large favorable enthalpy associated with tertiary structural folding in this pseudoknot.

Previous thermodynamic studies on the stability of the 58 nucleotide L11 rRNA fragment provide evidence for a phylogenetically conserved G-C·C base-triple, the formation of which greatly stabilizes the tertiary structure of the molecule (Conn *et al.*, 1998). Examination of the pH dependence of the L11 rRNA tertiary structure unfolding suggests that, in contrast to the BWYV pseudoknot, a protonated cytosine base is not involved in this interaction. However, significant pH-dependence is induced in the non-cognate U-A·C<sup>+</sup> base-triple which exhibits maximal tertiary structural stability at low pH (Conn *et al.*, 1998). Elimination of the base-triple upon substitution of a C-G·U destroys tertiary structure formation in this RNA while the non-cognate U-A·U base-triple is effectively as stabilizing as the wild-type base-triple. The effect of these substitutions in the L11 rRNA and their dependence on pH contrasts sharply with the thermodynamic behavior of the exactly analogous substitution mutants in the BWYV pseudoknot, indicative of two structurally distinct base-triples which play unique roles in stabilizing their respective folded RNA structures (Su *et al.*, 1999; Conn *et al.*, 1999). The stabilizing effect of the L11 base-triple (Conn *et al.*, 1998) includes a significant enthalpic component which is presumably derived from its position in the structure (Conn *et al.*, 1999) where it forms the top of a stack of three triple base-pairs in the core of the molecule. In the BWYV pseudoknot, the additional stabilization induced by protonation is almost entirely entropically derived, consistent with the idea that protonation of C8 is largely modulating the loop closing energetics for the pseudoknot folding, rather than inducing multiple new sites of stabilizing interactions. This is fully consistent with other studies on RNA pseudoknots where the nature of the nucleotide(s) in loop 1 perturbs the global stability of these molecules in the absence of large changes in the net enthalpy of stabilization (Theimer *et al.*, 1998; Theimer & Giedroc, 1999; P.L.N. & D.P.G., unpublished results).

An algorithm based on polymer theory has recently been published which approximates loop free energy penalties for pseudoknots and therefore enables the prediction of pseudoknot formation from nucleotide sequence (Gultyaev *et al.*, 1999). This approximation is obviously based on the assumption that the stability of a pseudoknot is

derived exclusively from pairs of helical stems connected by flexible loops and therefore neglects any stabilizing enthalpic contributions from loop-stem interactions. These predictions appear to be reasonable first approximations for pseudoknot stabilities that lack defined tertiary structural interactions in cases where an experimental determination of  $\Delta G_{37}^{\circ}$  is available, e.g. for the T4 and T2/T6 phage gene 32 autoregulatory pseudoknots (Theimer *et al.*, 1998; Nixon & Giedroc, 1998) and for the mIAP (Theimer & Giedroc, 1999) and MMTV (Theimer & Giedroc, 2000) frameshifting pseudoknots. However, some of this agreement may well be fortuitous since measurable perturbations in global stability associated with substitutions of loop nucleotides have been documented to occur in the T2, T4, and mIAP pseudoknots (Nixon & Giedroc, 1998; Theimer & Giedroc, 1999). The BWYV pseudoknot appears to be unique in that it has a large number of crystallographically defined tertiary contacts (Su *et al.*, 1999). Our experiments show that the stability of this RNA derived from calorimetry at pH 6.0 is  $-16(\pm 1) \text{ kcal mol}^{-1}$ , significantly more negative than predictions afforded by polymer theory ( $-6.3 \text{ kcal mol}^{-1}$ ), which actually argue against pseudoknot formation given the predicted and experimentally determined stability for helical stem 1. Thus, while the approximation method may be applicable for pseudoknots with flexible loops and few loop-stem interactions, it will obviously fail in situations where substantial enthalpic stabilization derived from loop-stem interactions is present.

Apart from the implications that this work has on our understanding of the origin of the stability of frameshifting pseudoknots, the functional importance of these highly stabilizing interactions has yet to be tested. Of the retroviral and plant viral pseudoknots that stimulate  $-1$  frameshifting, this particular structure stimulates a relatively low efficiency of frameshifting ( $\approx 1\%$ ) (Miller *et al.*, 1995). This may be due in part to the BWYV slippery sequence (G GGA AAC) which has been shown to function at relatively lower levels *in vivo* in *Escherichia coli* and *in vitro* in wheat germ and rabbit reticulocyte lysates relative to other slippery sequences. In *E. coli*, the BWYV pseudoknot is capable of supporting five percent frameshifting when the slip site is substituted with the *E. coli* preferred A AAA AAG site, indicating that the G GGA AAC site may not provide an optimal context for frameshifting in non-native systems (Garcia *et al.*, 1993). The relative frameshifting efficiencies of the wild-type and other mutant RNA pseudoknots have yet to be measured in the same sequence context at frameshifting efficiencies that would be optimal for comparison. The studies presented here will aid in the mechanistic interpretation of these functional assays since they provide a quantitative determination of the extent to which mutant RNAs are destabilized relative to the wild-type RNA, as well as insight into the

energetics of the pseudoknot unfolding reaction coordinate.

## Materials and Methods

### RNA synthesis and purification

RNAs were generated by *in vitro* transcription from synthetic templates utilizing phage T7 RNA polymerase and purified as described (Theimer *et al.*, 1998; Nixon & Giedroc, 1998). In brief, RNAs were purified by denaturing PAGE then desalted on an Alltech C18 cartridge prior to dialysis against a minimum of three buffer changes of  $K_{50}M_{10}$  buffer (50 mM KCl, 10 mM Mops (pH 7.0)) with the first dialysis buffer change containing 0.05 M EDTA.

### Optical spectroscopy and data analysis

Prior to thermal denaturation, RNAs were diluted into the appropriate buffer to 1–3  $\mu$ M RNA and heated to 65 °C for five minutes. The RNAs were then allowed to cool to room temperature for 45 minutes before loading into capped cuvettes. The RNAs were subjected to thermal denaturation monitored on a Cary 1 UV/Vis spectrophotometer operating in double beam mode. Percentage transmittance data were collected as a function of temperature at the rate of 0.3 deg. per minute and were found to be thermodynamically reversible under these conditions. Data were converted to absorbance and the first derivative with respect to temperature and fit to a multiple sequential interacting transition model as described using the t-melt fitting program (Theimer *et al.*, 1998; Nixon & Giedroc, 1998; Theimer & Giedroc, 1999).

### DSC and data analysis

DSC scans were acquired utilizing a Microcal VP-Differential Scanning Calorimeter. Samples were prepared by diluting concentrated RNA stocks as prepared above into ddH<sub>2</sub>O to give >30  $\mu$ M. This sample was then dialyzed at 4 °C for ten hours against one liter of the appropriate buffer. Following dialysis, RNA concentration was determined by making parallel serial dilutions of the RNA into final dialysis buffer to return the total observed absorbance to the linear range. Alkaline hydrolysis by the addition of 40  $\mu$ l of 2 M KOH to the diluted sample was used to correct for the hyperchromic effect. RNA sample concentrations were corrected for dilution and the exact concentration determined utilizing the predicted  $A_{260}$  for each individual RNA. The final dialysis buffer was used as the reference to the RNA sample during the experimental run, a temperature ramp from 5 to 120 °C at the rate of 1 deg. C per minute.

DSC scans were analyzed utilizing the Origin DSC software from Microcal Inc. This software utilizes a Levenburg-Marquadt least squares minimization to determine the best fit for a given set of experimental data. Prior to analysis, DSC reference scans were subtracted from DSC sample scans to give reference subtracted data. The heat capacity curve thus generated was then normalized to the RNA sample concentration to generate a  $C_p$  versus temperature curve. The resulting heat capacity curve was then subjected to baseline interpolation using a linear baseline approximation method and fit to an appropriate number of sequential

interacting transitions to return  $\Delta H_{vH,i}$  and  $t_{m,i}$ . The area from the baseline to the  $C_p$  curve was integrated to give the  $\Delta H_{cal}$ , the total enthalpy of denaturation. The sequential interacting transition model used by the Origin software is essentially identical to the one used by the t-melt program (Theimer & Giedroc, 1999).

### Fitting criteria

Assignment of an appropriate number of unfolding transitions for the fitting model was based on the following criteria. A minimum of two unfolding transitions are expected to be observed derived from the helix to coil transitions for the two crystallographically observed stems. For the wild-type BWYV RNA, modeling of the DSC data as two sequential unfolding transitions returns a total van't Hoff unfolding enthalpy of 103 kcal mol<sup>-1</sup> at pH 7.0 in 0.5 M K<sup>+</sup>, much less than the model independent calorimetric determination of 121 kcal mol<sup>-1</sup>. Introduction of a third transition in the fitting model results in a tenfold improvement in  $\chi^2$  and accompanying increase in the randomness of the residuals, with a total returned  $\Delta H_{vH}$  equal to  $\Delta H_{cal}$  (Table 1). These three transition fits converge to the same values of  $\Delta H_{vH}$  and  $t_m$  independent of starting point in the absence of any fitting constraints. Modeling the DSC data as four sequential unfolding transitions improves the returned values of  $\chi^2$  by approximately 20%, but the fits to four transitions are degenerate with multiple sets of returned values for  $\Delta H_{vH}$  and  $t_m$  returning equivalent values for  $\chi^2$ . When this same approach is applied to the optical data, a twofold improvement in  $\chi^2$  is observed from the use of three, rather than two, transitions. Again, introduction of a fourth transition results in divergent fits to the data in the absence of fitting constraints with no apparent improvement of  $\chi^2$  while a three transition model reproducibly converges to a unique fit from all starting points without fitting constraints.

In all cases examined, the calorimetric and optical melting profiles were best described by three sequential interacting transitions as outlined above. The selection and application of the three transition unfolding model is based on the smallest number of unfolding transitions that produce a minimal  $\chi^2$  value associated with unique fits to the data independent of starting parameters in the absence of fitting constraints.

### pH dependence studies

Buffer stock solutions were prepared from ACS-grade buffer salts (Sigma). All buffers were prepared in 0.5 M KCl and 0.010 M buffer component. The buffers used were: Mes (pH 5.5 and pH 6.0), Mops (pH 6.5 and pH 7.0), Hepes (pH 7.5 and pH 8.0), Epps (pH 8.5), Ches (pH 9.0) similar to a previous study on the pH dependence of base-triple in solution (Conn *et al.*, 1998).

### Monovalent salt concentration dependence of RNA unfolding

Buffers used for the determination of the monovalent salt concentration dependence were made using Mops (ACS grade, Sigma). An appropriate amount of salt, NH<sub>4</sub>Cl, KCl or NaCl (ACS grade, Sigma), was added to a stock solution of Mops (pH 7.0) to give the desired final concentrations of the metal salt. Since there was no systematic variation in  $\Delta H$  of unfolding associated with monovalent ion concentration or type, values for  $\Delta H$

used to calculate  $\Delta n$  were calculated by averaging the  $\Delta H$  values returned from the fits for each transition over all metal concentrations and types. The actual  $\Delta H$  values used were 30.1, 27.1 and 52.3 kcal mol<sup>-1</sup> for transitions 1, 2 and 3, respectively.

## Note added in proof

While this manuscript was under review, an extensive *in vitro* and *in vivo* mutational analysis of the frameshifting efficiencies for the BWYV pseudoknot located six nucleotides downstream of an efficient, non-cognate slippery sequence was reported (Kim *et al.* (1999) *Proc. Natl Acad. Sci.* **96**, 14234-14239). It was found that specific nucleotide substitutions which thermodynamically destabilize the native C8<sup>+</sup>·G12-C26 base triple and the loop 2-stem 1 triplex structure result in loss of function. In particular, the identity of the nucleotides comprising the C8<sup>+</sup>·G12-C26 base-triple, as well as nucleotides A23, A24 and A25 were found to be critical for activity. The functional effect of mutation of the G12-C26 base-pair to an A12-U26 base-pair, by itself or in the context of substitution of C8 with U8, as studied here, was not investigated in these studies.

## Acknowledgments

We thank Mr Brian Cannon for highly purified T7 RNA polymerase. He was supported by a Howard Hughes Medical Institute Undergraduate Biological Sciences Education Program Grant (71195-535101). This work was supported by NIH grant (AI40187) to D.P.G. and David W. Hoffman and a grant from the Robert A. Welch Foundation (A-1295). The calorimetry instrumentation was obtained with partial funding provided by the Texas Agricultural Experiment Station and an NIH grant (GM42569) to D.P.G.

## References

- Breslauer, K. J. & Sturtevant, J. M. (1977). A calorimetric investigation of single-stranded base stacking in the ribo-oligonucleotide A7. *Biophys. Chem.* **7**, 205-209.
- Brierley, I., Digard, P. & Inglis, S. C. (1989). Characterization of an efficient coronavirus ribosomal frameshifting signal: requirement for an RNA pseudoknot. *Cell*, **57**, 537-547.
- Cate, J. H., Gooding, A. R., Podell, E., Zhou, K., Golden, B. L., Kundrot, E. E., Cech, T. R. & Doudna, J. A. (1996). Crystal structure of a group I ribozyme domain: principles of RNA packing. *Science*, **273**, 1678-1685.
- Chen, X., Kang, H., Shen, L. X., Chamorro, M., Varmus, H. E. & Tinoco, I., Jr (1996). A characteristic bent conformation of RNA pseudoknots promotes -1 frameshifting during translation of retroviral RNA. *J. Mol. Biol.* **260**, 479-483.
- Conn, G. L., Gutell, R. R. & Draper, D. E. (1998). A functional ribosomal RNA tertiary structure involves a base-triple interaction. *Biochemistry*, **37**, 11980-11988.
- Conn, G. L., Draper, D. E., Lattman, E. E. & Gittis, A. G. (1999). Crystal structure of a conserved ribosomal protein-RNA complex. *Science*, **284**, 1171-1174.
- Dinman, J. D., Ruiz-Echevarrai, M. J., Czaplinski, K. & Peltz, S. W. (1997). Peptidyl-transferase inhibitors have antiviral properties by altering programmed -1 ribosomal frameshifting efficiencies: development of model systems. *Proc. Natl Acad. Sci. USA*, **94**, 6606-6611.
- Du, Z., Giedroc, D. P. & Hoffman, D. W. (1996). Structure of the autoregulatory pseudoknot within the gene 32 messenger RNA of bacteriophages T2 and T6: a model for a possible family of structurally related RNA pseudoknots. *Biochemistry*, **35**, 4187-4198.
- Du, Z., Holland, J. A., Hansen, M. R., Giedroc, D. P. & Hoffman, D. W. (1997). Base-pairings within the RNA pseudoknot associated with the Simian retrovirus-1 *gag-pro* frameshift site. *J. Mol. Biol.* **270**, 464-470.
- Farabaugh, P. J. (1993). Programmed translational frameshifting. *Microbiol. Rev.* **60**, 103-134.
- Filimonov, V. V. & Privalov, P. L. (1978). Thermodynamics of base interaction in (A)<sub>n</sub> and (A·U)<sub>n</sub>. *J. Mol. Biol.* **122**, 465-470.
- Fresco, J. R., Klotz, L. C. & Richards, E. G. (1963). A new spectroscopic approach to the determination of helical secondary structure in ribonucleic acids. *Cold Spring Harbor Symp. Quant. Biol.* **28**, 83-90.
- Garcia, A., van Duin, J. & Pleij, C. W. A. (1993). Differential response to frameshift signals in eukaryotic and prokaryotic translational systems. *Nucl. Acids Res.* **21**, 401-406.
- Gesteland, R. F. & Atkins, J. F. (1996). RECODING: dynamic reprogramming of translation. *Annu. Rev. Biochem.* **65**, 741-768.
- Gluick, T. C. & Draper, D. E. (1994). Thermodynamics of folding of a pseudoknotted mRNA fragment. *J. Mol. Biol.* **241**, 246-262.
- Gluick, T. C., Wills, N. M., Gesteland, R. F. & Draper, D. E. (1997). Folding of an mRNA pseudoknot required for stop codon readthrough: effects of mono- and divalent ions on stability. *Biochemistry*, **36**, 16173-16186.
- Gulyaev, A. P., Van Batenburg, F. H. D. & Pleij, C. W. A. (1999). An approximation of loop free energy values of RNA H-pseudoknots. *RNA*, **5**, 609-627.
- Holland, J. A., Hansen, M. R., Du, Z. & Hoffman, D. W. (1999). An examination of coaxial stacking of helical stems within a pseudoknot motif: the gene 32 messenger RNA pseudoknot of bacteriophage T2. *RNA*, **5**, 257-271.
- Hung, M., Patel, P., David, S. & Green, S. R. (1998). Importance of ribosomal frameshifting for human immunodeficiency virus type 1 particle assembly and replication. *J. Virol.* **72**, 4819-4824.
- Kang, K. S. (1998). Direct structural evidence for formation of a stem-loop structure involved in ribosomal frameshifting in human immunodeficiency virus type 1. *Biochim. Biophys. Acta*, **1397**, 73-78.
- Kolk, M. H., van der Graff, M., Wijmenga, S. S., Pleij, C. W. A., Heus, H. A. & Hilbers, C. W. (1998). NMR structure of a classical pseudoknot: interplay of single- and double-stranded RNA. *Science*, **280**, 434-438.
- Laing, L. G. & Draper, D. E. (1994). Thermodynamics of RNA folding in a conserved ribosomal RNA domain. *J. Mol. Biol.* **237**, 560-576.

- Laing, L. G., Gluick, T. C. & Draper, D. E. (1994). Stabilization of RNA structure by Mg ions: specific and non-specific effects. *J. Mol. Biol.* **237**, 577-587.
- Matsufuji, S., Matsufuji, T., Wills, N. M., Gesteland, R. F. & Atkins, J. F. (1996). Reading two bases twice: mammalian antizyme frameshifting in yeast. *EMBO J.* **15**, 1360-1370.
- Miller, W. A., Dinesh-Kumar, S. P. & Paul, C. P. (1995). Luteovirus gene expression. *Crit. Rev. Plant Sci.* **14**, 179-211.
- Nixon, P. L., . & Giedroc, D. P. (1998). Equilibrium unfolding (folding) pathway of a model H-type pseudoknotted RNA: the role of magnesium ions in stability. *Biochemistry*, **37**, 16116-16129.
- Nixon, P. L., Theimer, C. A. & Giedroc, D. P. (1999). Thermodynamics of stabilization of RNA pseudoknots by cobalt(III) hexaammine. *Biopolymers*, **50**, 443-458.
- Pleij, C. W. A., Rietveld, K. & Bosch, L. (1985). A new principle of RNA folding based on pseudoknotting. *Nucl. Acids Res.* **13**, 1717-1731.
- Rettberg, C. C., Prere, M. F., Gesteland, R. F., Atkins, J. F. & Fayet, O. (1999). A three-way junction and constituent stem-loops as the stimulator for programmed: 1 frameshifting in bacterial insertion sequence IS911. *J. Mol. Biol.* **286**, 1365-1378.
- Saenger, F. (1984). *Principles of Nucleic Acid Structure*, Springer-Verlag, New York.
- Silverman, S. K. & Cech, T. R. (1999). Energetics and cooperativity of tertiary hydrogen bonds in RNA structure. *Biochemistry*, **38**, 8691-8702.
- Su, L., Chen, L., Egli, M., Berger, J. M. & Rich, A. (1999). Minor groove RNA triplex in the crystal structure of a ribosomal frameshifting viral pseudoknot. *Nature Struct. Biol.* **6**, 285-292.
- Szewczak, A. A., Podell, E. R., Bevilacqua, P. C. & Cech, T. R. (1998). Thermodynamic stability of the P4-P6 domain RNA tertiary structure measured by temperature gradient gel electrophoresis. *Biochemistry*, **37**, 11162-11170.
- Theimer, C. A. & Giedroc, D. P. (1999). Equilibrium unfolding pathway of an H-type RNA pseudoknot which promotes programmed-1 ribosomal frameshifting. *J. Mol. Biol.* **289**, 1283-1299.
- Theimer, C. A. & Giedroc, D. P. (2000). Contribution of the intercalated adenosine at the helical junction to the stability of the gag-pro frameshifting pseudoknot from mouse mammary tumor virus. *RNA*, In the press.
- Theimer, C. A., Wang, Y., Hoffman, D. W., Kirsch, H. M. & Giedroc, D. P. (1998). Non-nearest neighbor effects on the thermodynamics of unfolding of a model mRNA pseudoknot. *J. Mol. Biol.* **279**, 545-564.
- Wyatt, J. R., Puglisi, J. D. & Tinoco, I., Jr (1990). RNA pseudoknots. Stability and loop size requirements. *J. Mol. Biol.* **214**, 455-470.
- Xia, T., SantaLucia, J., Jr, Burkard, M. E., Kierzek, R., Schroeder, S. J., Jiao, X. & Turner, D. H. (1998). Thermodynamic parameters for an expanded nearest-neighbor model for formation of RNA duplexes with Watson-Crick base-pairs. *Biochemistry*, **37**, 14719-14735.

Edited by I. Tinoco

(Received 19 October 1999; received in revised form 13 December 1999; accepted 13 December 1999)